JOURNAL OF RENEWABLE ENERGY AND SMART GRID TECHNOLOGY

Vol. 20, No. 2, July-December 2025

A Model for Estimating Hourly Erythemal UV Radiation from Satellite Data

Pranomkorn Choosri[1*], Noppamas Pratummasoot[2], Sumaman Buntoung[3]

[1]Department of Biomedical Engineering, College of Health Sciences, Christian University of Thailand, Nakhon Pathom 73000, Thailand

[2]Applied Physics Program, Faculty of Science and Technology, Valaya Alongkorn Rajabhat University under the Royal Patronage, Pathum Thani 13180, Thailand

[3]Department of Physics, Faculty of Science, Silpakorn University, Nakhon Pathom 73000, Thailand

***Corresponding author's email**: pranomkorn.aum@gmail.com

Article info:

Received: 18 May 2025
Revised: 11 July 2025
Accepted: 20 August 2025
DOI: 10.69650/rast.2025.262196

Keywords:

Erythema
Ultraviolet Radiation
Modeling
Meteorology
Satellite Data

ABSTRACT

Erythemal ultraviolet (EUV) irradiance, with a wavelength range of 280–400 nm, is associated with both health risks and physiological benefits. While moderate EUV exposure stimulates vitamin D synthesis—essential for bone health and immune function—excessive exposure can cause skin damage, ocular complications, and increased risk of skin cancer, highlighting the need for accurate UV monitoring. However, ground-based measurements remain limited due to the high cost of instrumentation. This study introduces a semi-empirical model for estimating hourly EUV irradiance in Thailand using meteorological and satellite data. The model was developed using cloud index, visibility, total column ozone, and the cosine of the solar zenith angle across four stations: Chiang Mai, Ubon Ratchathani, Nakhon Pathom, and Songkhla. The baseline model, constructed using data from 2016 to 2019, achieved a mean bias difference (MBD) of 3.57%, a root mean square difference (RMSD) of 21.80%, and an R^2 of 0.81. However, its performance declined in areas with high aerosol loading and low visibility, particularly in Chiang Mai, where seasonal biomass burning is prevalent. To improve accuracy, a modified model was developed by incorporating aerosol optical depth (AOD) at stations where such data were available. The enhanced model yielded an MBD of 6.18%, an RMSD of 15.16%, and an R^2 of 0.93. These results highlight the critical role of aerosols in UV attenuation and demonstrate the model's potential for scalable, cost-effective applications in UV risk assessment, especially in regions lacking high-resolution ground monitoring infrastructure.

1. Introduction

Ultraviolet radiation (UV) is part of the solar spectrum and consists of three bands i.e. UV-A (320-400 nm), UV-B (280-320 nm) and UV-C (100-280 nm). As stratospheric ozone can strongly absorb short wavelength radiation, all of UV-C cannot transmit to the earth's surface. Thus, only UV-A and part of UV-B reach the earth's surface with typical amounts of about 6.2% and 1.3% of the total energy from the sun respectively [1]. Although the total incident flux accounts for only a small fraction, approximately 8%, the high energy of the radiation may still damage living tissues [2-3]. The responses of organism to UV radiation are different, depending on wavelength. In this work, we are interested in UV radiation which has an effect on human skin. This radiation is usually called erythemal ultraviolet radiation or EUV. It covers the spectral UV irradiance between 280 – 400 nm weighted by the erythema action spectrum or erythemal response defined by Commission Internationale de l'Eclairage (CIE). Erythemal ultraviolet radiation (EUV) intensity can be calculated by integrating of the product of solar spectrum and erythemal response over 280 to 400 nm as follows:

$$EUV = \int_{280}^{400} R_{E\lambda} I_{\lambda} \, d\lambda \quad (1)$$

where EUV is the solar erythemal ultraviolet radiation in $W.m^{-2}$, $R_{E\lambda}$ is erythemal response in dimensionless, I_{λ} is solar spectrum in $W.m^{-2}$ and λ is wavelength in nm.

The strength of UV radiation depends on atmospheric components, particularly stratospheric ozone. The ozone layer filters UVC and UVB from reaching the atmosphere, but substances like chlorofluorocarbons (CFCs) have depleted it [4-5]. UV radiation reaches Earth's surface more. Besides ozone, clouds, dust, and atmospheric moisture can impact UV radiation intensity [6-7].

UV radiation, when administered in suitable quantities, facilitates the synthesis of vitamin D in the human body, prevents rickets in children, and is employed in medical therapies for disorders such as psoriasis and sterilization [8]. Nonetheless, excessive exposure can result in skin burns, erythema, and a heightened risk of skin cancer. It can also damage human eyes, resulting in disorders such as inflammation and cataracts [9].

Considering the benefits and risks associated with ultraviolet radiation, both researchers and the general public strive to monitor daily ultraviolet radiation levels to mitigate its potential hazards. Researchers have deployed instruments at various locations to monitor the intensity of ultraviolet radiation. Also they try to develop model for prediction these value such as Hu et al. (2008) [10] studied the influence of the clearness index on ultraviolet solar radiation at two high-altitude locations on the Tibetan Plateau: Lhasa and Haibei. The research examines the relationship between UV radiation, global solar radiation, optical mass, and atmospheric conditions. Lhasa has stronger yearly UV radiation than Haibei due to its altitude and lower aerosol and ozone levels. The study found that cloud cover attenuates global solar radiation more than UV radiation and raises the UV-to-global solar radiation ratio. Quantifying UV radiation-optical mass relationships revealed UV behavior under different air conditions. These findings help explain UV climate and UV radiation's ecological effects, especially in high-altitude places with distinct atmospheric circumstances. Choosri et al. (2017) [11] estimated monthly average hourly diffuse erythemal ultraviolet (EUV) radiation in Thailand under all sky conditions using an empirical model. The model included air mass, aerosol optical depth, and a satellite-derived cloud index, which matched ground-based data. Diurnal and seasonal diffuse EUV radiation maps generated by the model showed significant geographical and temporal variability influenced by cloud cover and solar zenith angle. These findings help explain UV radiation's distribution and potential effects on tropical ecosystems and health. Lamy et al. (2018) [12] used Bentham spectroradiometer readings and satellite observations to estimate Reunion Island's surface UV radiation (SUR). The island has higher SUR than comparable sites due to its tropical location, low ozone, and low aerosol concentration. UVI is estimated using the Tropospheric Ultraviolet and Visible (TUV) radiative transfer model under clear skies and pyranometer data during cloudy times. Ozone cross-sections and total column ozone greatly affect UVI estimates in SUR modeling, according to the study. Aerosol characteristics and alien solar spectra are also examined. The typical relative difference between predicted and observed data is 0.5%, with SBUV ozone data being most accurate. These findings improve tropical UVI parameterization for climate modeling and UV exposure risk assessments. García-Rodríguez et al. (2023) [13] examined UV erythemal irradiance (UVER) in Burgos, Spain, under various sky conditions using meteorological data from September 2020 to June 2022. Multilinear regression (MLR) and artificial neural networks (ANN) are used to model UVER using climatic factors, overcome the lack of UV sensors. ANN models outperform MLR with higher accuracy ($R^2 > 0.95$) and lower error (nRMSE < 15%), especially under clear skies. UVER/GHI peaked at noon and in summer, while cloud cover strongly attenuated it. The study found that ANN-based models can accurately estimate UVER from meteorological factors, which has implications for public health, climate studies, and solar energy. Buntoung et al. (2024) [14] used ground-based and satellite-based data to estimate monthly average hourly vitamin D–weighted solar UV radiation over Thailand. Ozone, cloud, aerosol, solar zenith angle, air mass, and extraterrestrial UV radiation are inputs. Numerous researchers have examined UV radiation changes or developed models using readily available atmospheric variables [3,15-21]. Thailand has four UV radiation monitoring stations in Chiang Mai, Ubon Ratchathani, Nakhon Pathom, and Songkhla. Each station represents a region in Thailand. For Chiang Mai, it is located at 98.98°E and 18.78°N, which displays the geographical characteristics of the northern region. The local climate is characterized by tropical savanna climate type Aw of the Köppen climate classification [22-23]. The southwest monsoon (May–October) has a significant impact on Chiang Mai, resulting in elevated humidity and substantial rainfall. The climate is pleasant during the Northeast Monsoon (November–February), which is characterized by dry air. Aerosols are an important component of climate science. Aerosols in Chiang Mai are produced by both natural and human-made sources. The concentrations of aerosols in Chiang Mai are subject to significant seasonal fluctuations [24-25]. Ubon Ratchathani is a province in the Isan region of northeastern Thailand, famous for its tropical climate, bending plateaus, and border with the Mekong River. One of Thailand's largest provinces, it is characterized by a combination of plains, rivers, forests, and hills. Ubon Ratchathani is located at 104.87°E and 15.25°N. Ubon Ratchathani experiences a tropical savanna climate (Aw), which is comparable to that of Chiang Mai. Ubon Ratchathani is affected by the influence of two primary monsoons: The Southwest Monsoon (May–October), which brings warm, moisture-laden air from the Indian Ocean, resulting in heavy rainfall, high humidity, and occasional flooding, particularly along the Mun and Mekong Rivers; and the Northeast Monsoon (November–February), which carries cool, dry air from China and Siberia, resulting in cooler temperatures, dry weather, and occasional cold waves during the winter months. Nakhon Pathom is a central province of Thailand, situated approximately 56 km west of Bangkok, at 13.82°N, 100.04°E. It is situated within the Chao Phraya River Basin and features a flat terrain that is characterized by agricultural lands, canals, and a few low-lying hills. Throughout the year, the climate and weather patterns of Nakhon Pathom are significantly influenced by the monsoon. The province, like much of central Thailand, is influenced by two primary monsoons: The Southwest Monsoon and the Northeast Monsoon. Songkhla is located at 7.2° N latitude and 100.6° E longitude. Songkhla is a coastal province in southern Thailand, located along the Gulf of Thailand. It is characterized by a tropical climate, which is characterized by consistently warm temperatures and significant rainfall throughout the year. The province is a site of various geographical features, including mountains, lakes, beaches, and islands [26-27].

Each station exhibits distinct climatic and geographical characteristics, as previously described. Although these four stations provide valuable data for EUV monitoring, their spatial coverage is insufficient to represent the entire country. Consequently, researchers have attempted to develop models using easily accessible and spatially comprehensive atmospheric data to estimate UV irradiance across broader areas. However, studies focusing specifically on the development of models for hourly or instantaneous UV radiation particularly erythemal ultraviolet remain limited in Thailand.

In response to this research gap, the present study introduces a semi-empirical model for estimating hourly EUV irradiance using commonly available meteorological and satellite-derived data. The model is designed to strike a balance between computational simplicity and scientific accuracy, making it suitable for use in regions with limited monitoring infrastructure. Given the high spatial and temporal variability of atmospheric constituents—particularly aerosols and clouds in tropical regions like Thailand—his approach enables scalable, low-cost, and regionally adaptable UV estimation across diverse environmental conditions.

Recent studies have underscored the critical role of aerosols in modulating UV radiation, especially in Southeast Asia, where seasonal biomass burning leads to sharp fluctuations in atmospheric transparency [28-30]. Integrating such variables into modeling

frameworks is increasingly important for improving spatial accuracy and supporting public health applications, such as UV exposure forecasting and environmental risk communication.

The objective of this study is to develop a semi-empirical model for estimating hourly EUV irradiance using satellite and meteorological parameters. The model aims to estimate EUV irradiance in areas lacking direct measurements, offering a cost-effective alternative to ground-based instruments. Moreover, the results obtained from the model can support public health initiatives by serving as a reference for UV exposure alerts and long-term risk assessments.

2. Data and Instruments

2.1 Ground-based measurement data

2.1.1 Erythemal ultraviolet irradiance

Hourly erythemal ultraviolet (EUV) irradiance was measured using UV biometers (Solar Light, model 501A) at four stations across Thailand, namely Chiang Mai (18.78°N, 98.98°E), Ubon Ratchathani (15.25°N, 104.87°E), Nakhon Pathom (13.82°N, 100.04°E) and Songkhla (7.20°N, 100.60°E) as shown in Fig. 1. The instruments are based on a filtered photodiode system and are regularly calibrated using a UV spectroradiometer (Bentham DMC150) at the Atmospheric Physics Laboratory, Silpakorn University [14]. Measurements were recorded every minute from 2016 to 2021, and converted to hourly averages using the method proposed by Webb et al. (2006) [31].

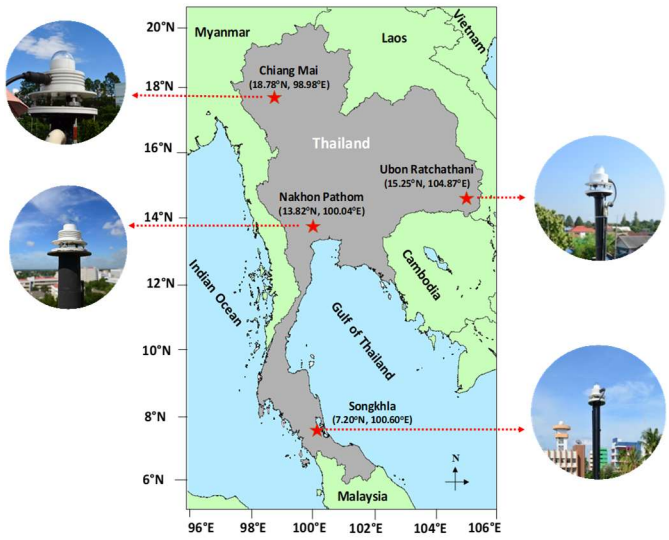

Fig. 1 Study area of erythemal ultraviolet irradiance in Thailand.

Data quality control followed the procedures outlined in Webb et al. (1988) [32] and Seckmeyer et al. (2007) [33]. The dataset was divided into two groups: 2016–2019 for analysis and model development, and 2020–2021 for model validation.

Example of monthly average hourly EUV irradiance data at four stations during 2016-2021 are shown in Fig. 2.

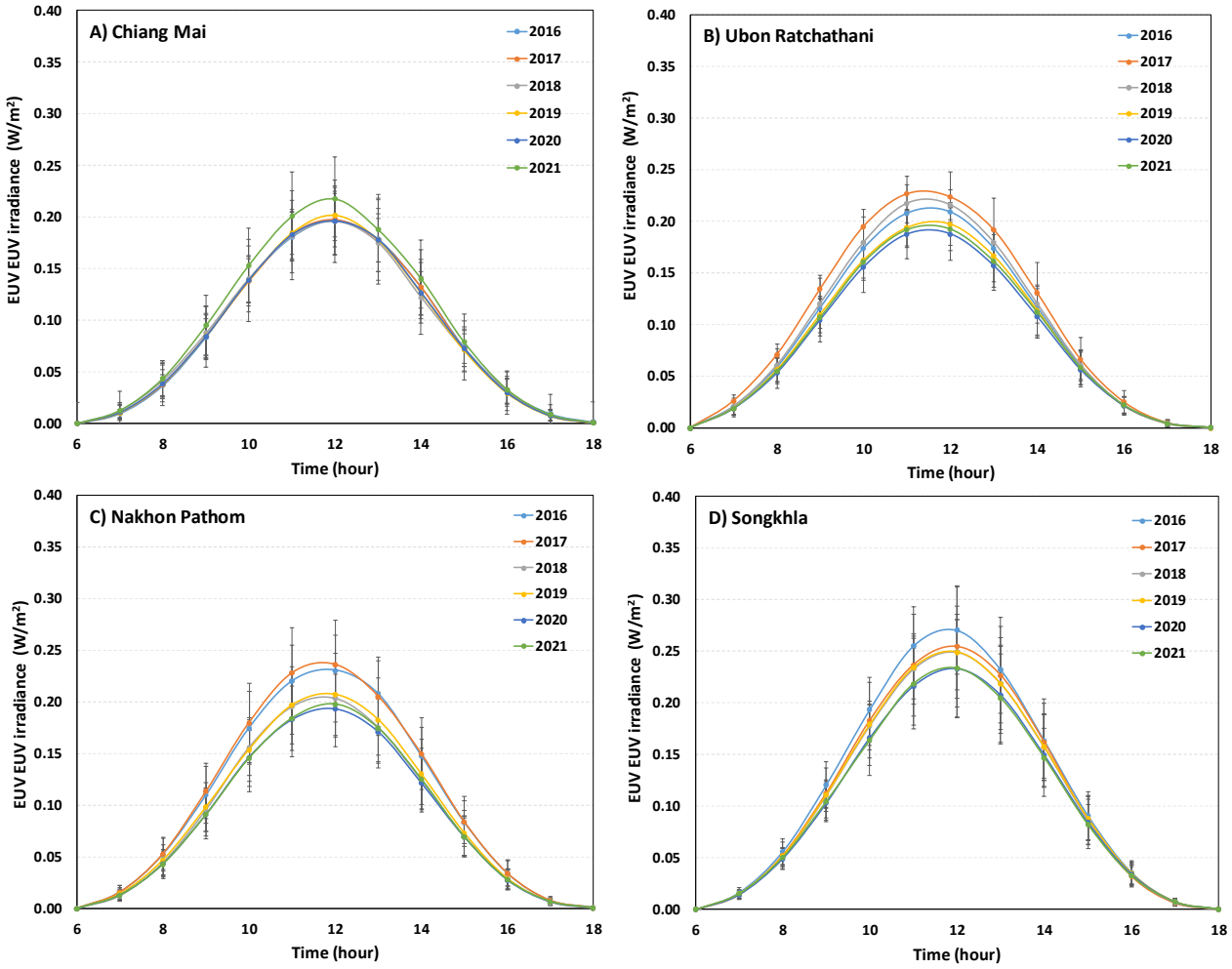

Fig. 2 Monthly average hourly erythemal ultraviolet (EUV) irradiance at four stations in Thailand (2016–2021). Each curve represents the hourly average across all days and years during the selected month.

Fig. 2 presents the monthly average of hourly EUV irradiance variations at four stations across Thailand during the 2016–2021 period. All stations exhibit a similar diurnal pattern, with irradiance increasing in the morning, peaking around solar noon (approximately 12:00 local time), and decreasing in the afternoon. The intensity of the monthly average hourly EUV irradiance ranges from 0.190 to 0.270 $W{\cdot}m^{-2}$. This trend reflects the influence of the solar zenith angle, which determines the atmospheric path length that solar radiation must traverse. Despite the overall uniform pattern, variations in peak intensities among the stations are evident. Chiang Mai and Nakhon Pathom tend to exhibit slightly higher EUV levels, likely due to drier conditions and reduced cloud cover during certain months. Conversely, Songkhla records lower peak values and a flatter curve, possibly influenced by persistent cloud cover and higher humidity typical of southern Thailand's tropical climate. These spatial and temporal variations highlight the importance of multi-parameter modeling that incorporates solar geometry, cloud index, and visibility to accurately estimate hourly EUV irradiance.

2.1.2 Visibility data

A useful surrogate for aerosol optical depth (AOD), which plays a critical role in modulating EUV irradiation through scattering and absorption mechanisms, is the visibility parameter [34-35]. Although direct AOD data from satellites or ground-based sun photometers are more accurate, such data are often limited in spatial and temporal coverage. In contrast, the Thai Meteorological Department consistently records visibility at more than 80 stations nationwide, providing broader geographic coverage and more continuous data availability. This widespread accessibility makes visibility a practical and readily available parameter for large-scale modeling, especially in areas lacking direct aerosol observations. Moreover, previous studies have shown that, under typical meteorological conditions in Southeast Asia, visibility correlates well with aerosol loading—particularly during haze episodes or biomass burning events. Therefore, incorporating visibility into the model not only enhances spatial applicability but also supports the estimation of EUV irradiation in regions where AOD data are unavailable or sparse.

In this work, visibility data were obtained from 86 meteorological stations distributed across Thailand, as illustrated in Fig. 3. These stations are operated by the Thai Meteorological Department (TMD), ensuring standardized procedures and consistent data quality nationwide. The data were recorded by professional meteorologists trained in observation techniques, adhering to established protocols defined by the World Meteorological Organization (WMO).

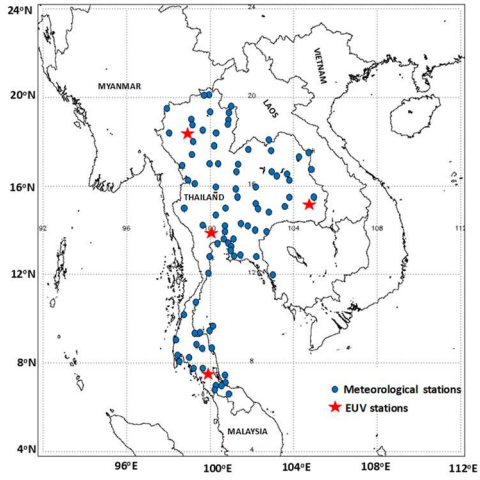

Fig. 3 location of meteorological stations in Thailand.

Visibility observations were taken every three hours at local time specifically at 01:00, 04:00, 07:00, 10:00, 13:00, 16:00, 19:00, and 20:00. These multiple time points throughout the day capture diurnal variation in aerosol conditions, which is essential for estimating EUV irradiance. The high spatial and temporal density of the data makes it particularly useful for interpolation across unsampled areas, enabling full spatial coverage of the country. Furthermore, the availability of long-term visibility records allows for integration with satellite data and supports reliable model development and validation over multiple years.

Hourly visibility data were generated using linear interpolation from 3-hourly observations, ensuring smooth temporal transitions and consistency with other hourly parameters in the model. This interpolation process enables the estimation of visibility values at locations where no meteorological stations are present, ensuring full spatial coverage for model application. The interpolation technique employed considers both spatial proximity and temporal trends, allowing for smoother and more realistic transitions between observation points.

By obtaining hourly visibility data, the model can more accurately reflect short-term variations in aerosol content, which is particularly important for capturing diurnal dynamics of EUV irradiance. This comprehensive dataset is essential for both model formulation and validation, as it allows consistent integration with other hourly parameters such as solar zenith angle, cloud index, and EUV measurements. Ultimately, the interpolated visibility data enhance the generalizability and scalability of the model, supporting its application in regions with limited or no ground-based observations.

Ground-based aerosol optical depth (AOD) measurements were obtained using sun photometers (CIMEL, model CE-318) installed at the same four stations as the EUV irradiance measurements. The instruments are part of the AERONET network and all raw data undergo quality control and are further processed into scientific variables from the AERONET central facility. Average daily values of wavelength exponent can be downloaded from the AERONET website at http://aeronet.gsfc.nasa.gov. In this work, the wavelength exponent at 340 nm were retrieved from 2016-2021 for each station. The relation between AOD and visibility as follow:

$$\beta = 0.589 - 0.068(VIS) + 0.0019(VIS)^2 \quad (2)$$

Angstrom's turbidity coefficient (β) was computed from visibility data (VIS) in km as follows [35].

Angstrom' s turbidity coefficient can be used to calculate AOD by using the Angstrom's equation [36] as follows:

$$AOD_{340} = \beta\lambda^{-\alpha} \quad (3)$$

where AOD_{340} is aerosol optical depth at 340 nm, α is wavelength exponent, λ is wavelength in μm and β is Angstrom's turbidity coefficient.

2.1.3 solar zenith angle

Air molecules, water vapor, clouds, and aerosols absorb and scatter solar radiation as it travels through the atmosphere. If the distance to the atmosphere or optical path is long, the solar radiation will be more attenuated. The path length is also related to air mass; as longer path lengths contain higher air mass. Generally, air mass is used in term of relative air mass [36] and relative air mass is usually estimated from solar zenith angle [θ_z]. Therefore, in order to estimate hourly EUV irradiance in this work, we used air mass in term of solar zenith angle.

Variation of hourly EUV irradiance depends on the solar path length. High path length during sunrise and sunset affect large extinction of solar radiation. While, small extinction at low path length leads high solar radiation intensity. Solar zenith angle can be calculating by Iqbal (1983) [36].

2.1.4 Extraterrestrial erythemal ultraviolet irradiance

Extraterrestrial EUV irradiance refers to the intensity of ultraviolet radiation—specifically within the erythemally effective wavelength range—received at the top of Earth's atmosphere, prior to any attenuation by atmospheric components such as ozone, aerosols, clouds, and gases. This radiation originates from the sun and represents the maximum potential UV exposure that could affect human skin in the absence of atmospheric filtering.

In scientific modeling, extraterrestrial EUV irradiance serves as a reference or baseline value for estimating surface-level UV exposure after accounting for atmospheric absorption and scattering. Its calculation depends on parameters such as the solar zenith angle, Earth–Sun distance, and the spectral distribution of solar radiation. A standard method for this calculation can be found in Iqbal (1983) [36].

2.2 Satellite data

2.2.1 Cloud index

Cloud index (n) represents the effect of clouds on erythemal ultraviolet irradiance. For cloud index data, these data can be obtained from Himawari-8 satellite. Himawari is owned by Japan Meteorological Agency (JMA). This satellite is located around 140.7°E above the equator and it was launched in 2016 to replace MTSAT. The Advanced Himawari Imager (AHI) sensor, a new payload forecast and aviation controls. For meteorology research, it comprises of a 16 channel multispectral imager to capture visible light and infrared images of the Asia-Pacific region. The Himawari system is scanned at a frequency of 10 minutes and the product comprises of 16 bands. The functions and specifications are improved from MTSATs. Color images will be derived by compositing three visible bands (blue: 0.47 µm; green: 0.51 µm; red: 0.64 µm). In this work, visible band for representation of cloud effected was used. The satellite data are 8-bit digital visible channel of Geostationary meteorology satellite. The data were collected between 8:30-16:30 during 2016-2021. Firstly, a digital count for each image (550x850 pixels) was converted to pseudo-reflectivity using a calibration table by satellite agency. The table consists of gray level value (0-255) and this value relates with earth-atmospheric albedo (0-1). The value was divided by the cosine of local solar zenith angle, and then earth-atmosphere reflectivity was obtained using these methods (Fig. 4). The formation of cloud index proposed by Cano et al. (1986) [37] as shown in Eq. 4

$$n = \frac{\rho_{EA} - \rho_{min}}{\rho_{max} - \rho_{min}} \quad (4)$$

where n is cloud index, ρ_{EA} is an earth-atmosphere reflectivity, ρ_{max} is maximum reflectivity and ρ_{min} is minimum reflectivity. To obtain ρ_{min} , the reflectivity image was selected at noontime and then compared pixel by pixel for each month. The minimum reflectivity of each pixel was selected and used as representative of ground surface albedo. In contrast, the maximum pixel value for each pixel was selected and represented as cloud reflectivity. Cloud index related to cloud cover, with high cloud index (close to 1) representing high cloud cover (close to 10) and vice-versa.

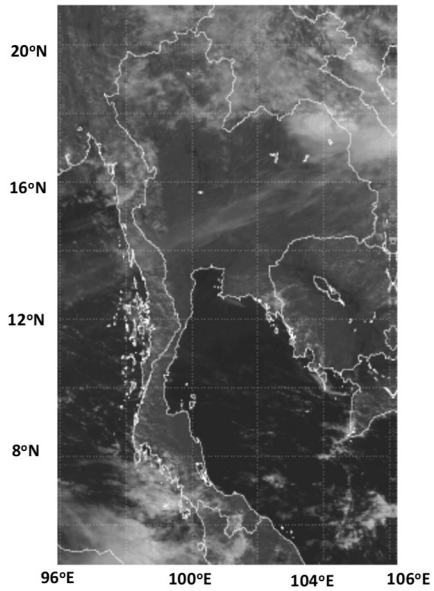

Fig. 4 An example of a navigated image.

2.2.2 Total column ozone

Total column ozone plays a crucial role in modulating erythemal ultraviolet irradiance by absorbing significant portions of UV-B radiation within the stratosphere. This protective effect is essential in limiting the biological impacts of solar radiation on human health. In this study, daily total column ozone data were acquired from the Ozone Monitoring Instrument (OMI) onboard NASA's Aura satellite. OMI provides high-quality, near-global measurements based on backscattered UV and visible radiation, with a spatial resolution of 0.25° x 0.25°, enabling region-specific analysis. The data were processed in Level 3e format and spatially matched to the locations of the ground stations. Given its well-established reliability, OMI-derived ozone measurements were selected to ensure robust and consistent input for the model. To align with the model's hourly resolution, the daily ozone data were interpolated accordingly. For the total column ozone data in this work, daily total column ozone was obtained from OMI/ AURA satellite during 2016-2021 (6 years). These data were accessed from https://acd-ext.gsfc.nasa.gov/anonftp/toms/omi/data/Level3e/ozone/.

For the data found that ozone concentration over Thailand typically ranges between 250 and 300 Dobson Units (DU), depending on the season and geographic location. Higher ozone values, around 280-300 DU, are commonly observed during the dry and summer seasons (March–May), when solar radiation is intense and atmospheric circulation enhances ozone formation. In contrast, values tend to decrease to about 250-270 DU during the rainy season (June–October), due to increased cloud cover and reduced photochemical activity. Regional variations also occur, with the northern part of Thailand often recording slightly higher ozone levels than southern regions.

3. Model formulation

In this study, a semi-empirical model was formulated to estimate hourly erythemal ultraviolet irradiance using both satellite-derived and ground-based meteorological parameters. The dataset used for model development covers diverse climatic and geographical conditions across Thailand, ensuring that the model captures regional variability in EUV irradiance. This station distribution ensures that the model can capture regional variability in EUV irradiance influenced by local weather conditions, aerosol loading, and cloud dynamics.

To ensure robust model construction and minimize the risk of overfitting, the complete dataset spanning 6 years (2016–2021) was divided into two subsets: one for model training and parameter fitting (2016–2019), and the other for independent model validation (2020–2021). This temporal separation allows for unbiased model evaluation and simulates real-world predictive performance, as supported by previous studies [38-39].

The foundational variable in this modeling approach is the solar zenith angle, which directly determines the path length of solar radiation through the atmosphere. Since EUV irradiance is strongly dependent on the angle at which sunlight penetrates the atmosphere, only data with a solar zenith angle less than 70° were selected. This threshold minimizes cosine error and ensures measurement reliability, as supported by Cordero et al. (2008) [40].

As a first step, hourly EUV irradiance was plotted against the cosine of the solar zenith angle for each station (Fig.5). The observed relationship exhibits a clear exponential trend, aligning with theoretical expectations from radiative transfer models. However, notable data scatter around the curve was also observed, particularly under cloudy or hazy conditions. This deviation highlights the influence of additional atmospheric variables namely, cloud index and visibility on EUV transmission.

In Fig. 5, shown the relationship between hourly EUV irradiance and the cosine of the solar zenith angle at 4 stations in Thailand. For all stations, EUV irradiance increases nonlinearly with increasing cosine of the solar zenith angle, confirming an exponential trend. This trend is consistent with the radiative transfer theory, where the path length of solar radiation shortens as the sun moves closer to zenith, thus reducing atmospheric attenuation. Despite the general exponential pattern, the data show significant scatter around the trend, especially during lower sun zenith angle (cosine of the solar zenith angle < 0.6). This variance can be defined to atmospheric components including cloud and aerosol, which are not included into this one-variable correlation.

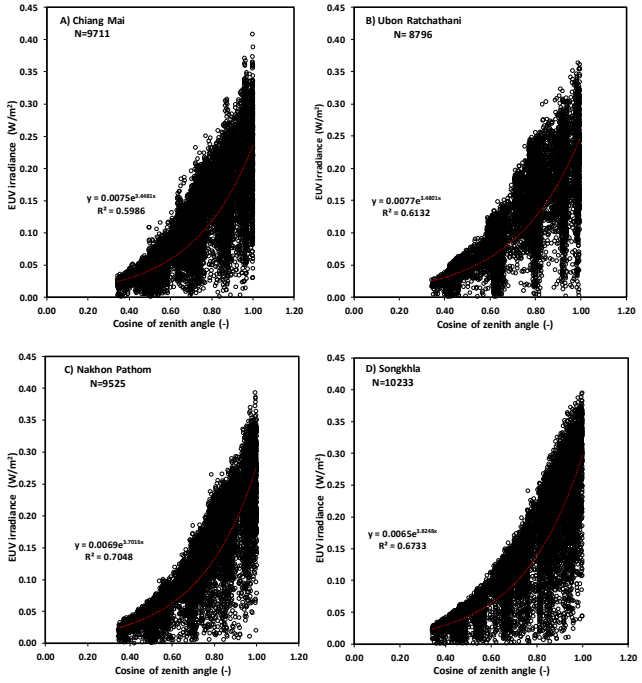

Fig. 5 The relation between the EUV data and cosine of solar zenith angle for A) Chiang Mai (CM), B) Ubon Ratchathani (UB), C) Nakhon Pathom (NP) and D) Songkhla (SK). N is total number of the data.

These variations generate attention to the need of other criteria like cloud index and visibility in the design of the model. Therefore, in the next step of the analysis, the difference between the measured EUV irradiance ($EUV_{measured}$) and the exponentially modeled EUV ($EUV_{model}(z)$) for each station was calculated. The difference was then plotted against the cloud index and visibility data. The relationship for both of these is linear relations, the statistics for each parameter, as shown in Fig.6 and Table 1-2.

Table 1 Statistic result of parameter with effect of cloud (n) on EUV.

Stations	$EUV_{measured} - EUV_{model}(z) = \beta_o + \beta_1 n$				
	β_o	β_1	t-stat	p-value	R
Chiang Mai	0.03134	-0.11423	-47.7439	<0.01	0.44
Ubon Ratchathani	0.03551	-0.17405	-74.9143	<0.01	0.62
Nakhon Pathom	0.03320	-0.18289	-89.5774	<0.01	0.68
Songkhla	0.04616	-0.21972	-103.488	<0.01	0.72

Table 2 Statistic result of parameter with effect of visibility (VIS) on EUV.

Stations	$EUV_{measured} - EUV_{model}(z) = \gamma_o + \gamma_1 VIS$				
	γ_o	γ_1	t-stat	p-value	R
Chiang Mai	-0.04018	0.004979	15.64721	<0.01	0.16
Ubon Ratchathani	-0.11063	0.012478	20.29864	<0.01	0.21
Nakhon Pathom	-0.05145	0.007112	20.51142	<0.01	0.21
Songkhla	-0.18335	0.018835	40.77891	<0.01	0.37

The regression coefficients ($\beta_o, \beta_1, \gamma_o, \gamma_1$) in both tables are statistically significant at the 99% confidence level, as indicated by p-values less than 0.01 and t-statistic values exceeding ±2.576 [39]. These results confirm that the relationships between cloud index, visibility, and EUV irradiance are not due to random variation, but represent statistically significant atmospheric influences on UV radiation.

As shown in Fig. 6, a comparative analysis across the four monitoring stations—Chiang Mai, Ubon Ratchathani, Nakhon Pathom, and Songkhla—reveals region-specific patterns in model deviation ($EUV_{measured} - EUV_{model}(z)$)under varying atmospheric conditions. These trends are further supported by the statistical data in Tables 1 and 2, which show that both cloud index and visibility significantly affect EUV variation. For instance, Songkhla consistently presents low deviation under conditions of high humidity and persistent cloud cover. This is consistent with its location in southern Thailand near the ocean, where clouds and rainfall occur throughout much of the year, and maritime aerosols contribute to reduced irradiance. Conversely, Chiang Mai shows the highest deviation during periods of low visibility, likely due to seasonal biomass burning, yet exhibits minimal impact from cloud cover and visibility overall. This is attributable to its inland geography, relatively dry climate, and the dominance of fine-mode aerosols. Ubon Ratchathani demonstrates marked variability in both cloud cover and visibility, while Nakhon Pathom shows relatively stable model performance across all variables. These findings collectively underscore the importance of incorporating localized atmospheric parameters—such as cloud index, visibility, and aerosol characteristics—into EUV estimation models to enhance their spatial accuracy and robustness.

The physical model includes atmospheric parameters such as aerosols, clouds, ozone, and air mass, based on the information in Iqbal (1983) [36]. Therefore, we proposed a simple semi-empirical model similar to the Iqbal model, which is a straightforward formula, not complicated.

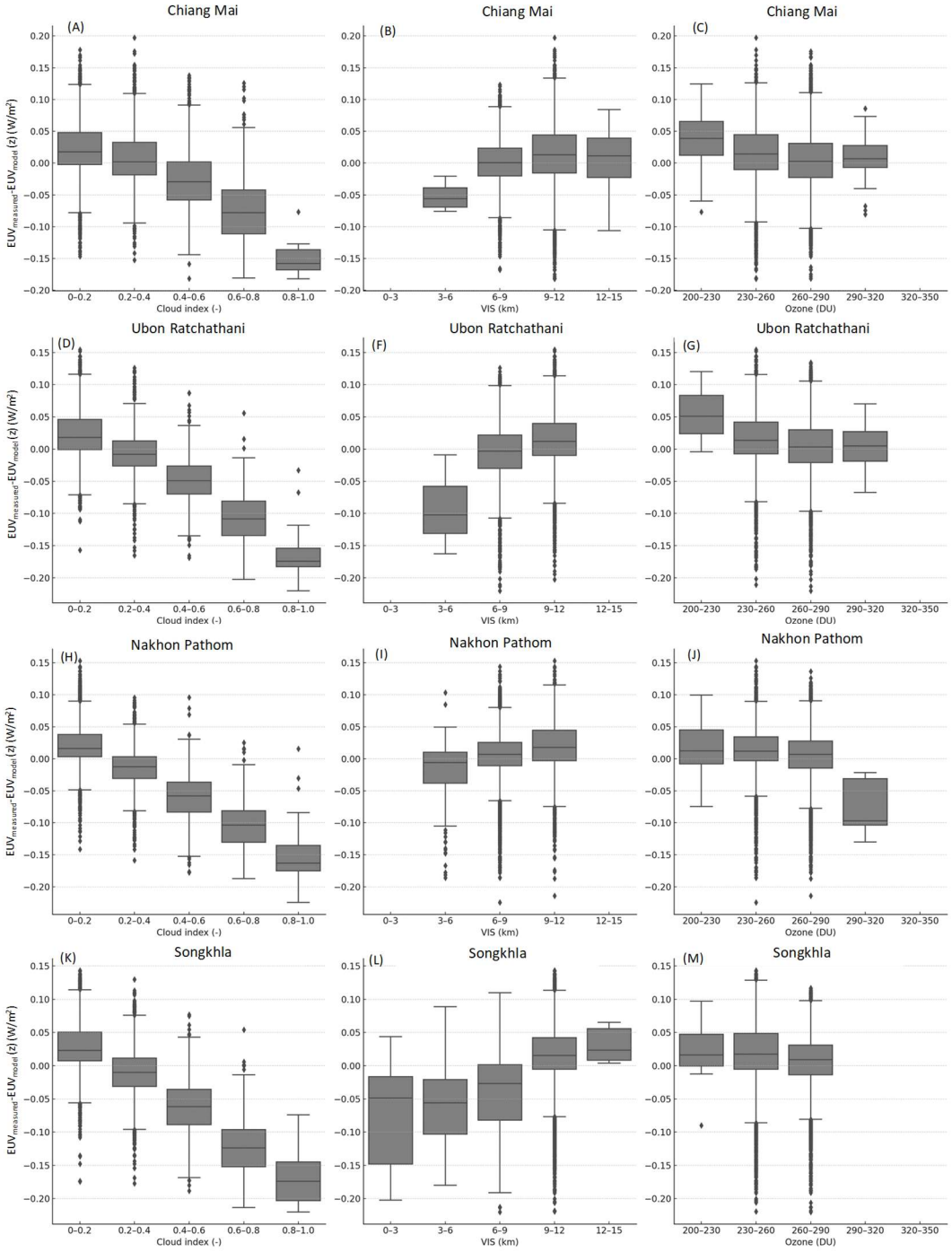

Fig 6. Comparison of model deviation ($EUV_{measured} - EUV_{model}(z)$) under varying atmospheric conditions across four monitoring stations in Thailand.

The presented model has the following form:

$$EUV = a_0 EUV_0 \, exp(\, a_1 VIS + a_2 n + a_3 O_z + a_4 \cos z) + a_5 \quad (5)$$

Where EUV is hourly erythemal ultraviolet irradiance in W.m^{-2}, EUV_o is hourly extraterrestrial erythemal ultraviolet irradiance in W.m^{-2}, $cos\ \theta_z$ is cosine of solar zenith angle , n is cloud index, O_z is total column ozone in DU and $a_o, a_1, \ldots, a_5$ are regression constants obtained statistic program as result shown in Table 3.

From Table 3, depict a high t-statistic related to high correlation and a low P-value. These statistical parameters indicated that the values of coefficients have a relationship with a level of significance at 99% [41]. Therefore, we can use all coefficients to estimate the erythemal ultraviolet irradiance for the entry area.

Table 3 Regression coefficients between EUV and their respective parameters. Coefficients have been obtained from Eq. 5 (R is correlation coefficient and N is total number of data).

Coef.	Value	t-stat	p-value	R	N
a_0	0.014309	36.494	<0.001	0.92	38265
a_1	0.057646	72.385			
a_2	-0.990261	-105.361			
a_3	-0.004162	-40.727			
a_4	1.455262	62.434			
a_5	-0.033050	-25.386			

Note: p-values and correlation coefficients correspond to individual regression parameters in the exponential model.

In this work, a modified version of the model incorporating AOD was applied to stations where aerosol optical depth measurements were available. The modified model has the following form:

$$EUV = a_0 EUV_0 \, exp(a_1 AOD + a_2 VIS + a_3 n + a_4 O_z + a_5 \cos z) + a_6 \quad (6)$$

Where EUV is hourly erythemal ultraviolet irradiance in W.m^{-2}, EUV_o is hourly extraterrestrial erythemal ultraviolet irradiance in W.m^{-2}, $cos\ \theta_z$ is cosine of solar zenith angle , n is cloud index, O_z is total column ozone in DU, AOD_{340} is aerosol optical depth at 340 nm and $a_o, a_1, \ldots, a_6$ are regression constants obtained statistic program as result shown in Table 4.

Table 4 Regression coefficients between EUV and their respective parameters. Coefficients have been obtained from Eq. 6 (R is correlation coefficient and N is total number of data).

Coef.	Value	t-stat	p-value	R	N
a_0	0.014462	35.0073	<0.001	0.97	3990
a_1	-0.238315	-80.1634			
a_2	0.051149	64.1800			
a_3	-0.280279	-21.4171			
a_4	-0.003851	-35.1104			
a_5	1.482060	58.8198			
a_6	-0.027874	-19.3956			

Note: p-values and correlation coefficients correspond to individual regression parameters in the exponential model.

Table 4 illustrates a low P-value and a high t-statistic, which are indicative of a high correlation. These statistical parameters suggested that the coefficient values are associated with a level of significance of 99% [41]. Consequently, the hourly EUV irradiance at four stations can be estimated by utilizing all coefficients.

Statistical analyses for the evaluation of the semi-empirical model performance are root mean square difference (RMSD) and mean bias difference (MBD) as described in Eq. (7) and (8).

$$RMSD(\%) = \frac{\sqrt{\frac{\sum_{i=1}^{n}\left(EUV_{i,mod} - EUV_{i,meas}\right)^2}{n}}}{\frac{\sum_{i=1}^{n} EUV_{i,meas}}{n}} \times 100 \quad (7)$$

$$MBD(\%) = \frac{\frac{\sum_{i=1}^{n}\left(EUV_{i,mod} - EUV_{i,meas}\right)}{n}}{\frac{\sum_{i=1}^{n} EUV_{i,meas}}{n}} \times 100 \quad (8)$$

Where $EUV_{i,mod}$ is EUV from the semi-empirical model, $EUV_{i,meas}$ is EUV from ground-based measurements and n is total number of the data.

4. Results and discussion

4.1 Baseline Model Validation

For model validation, the dependent hourly data namely, EUV, visibility, cloud index and total ozone column from 2020-2021 were selected. The modeled EUV value at four stations was estimated by Eq. 5 with regression coefficients a_o, a_1, a_2, a_3, a_4 and a_5. Fig. 5. compares the calculated and measured hourly EUV irradiance.

Fig. 7, the comparison between modeled and observed hourly EUV irradiance at each of the four stations, namely Chiang Mai, Ubon Ratchathani, Nakhon Pathom, and Songkhla reveals distinct differences in model performance.

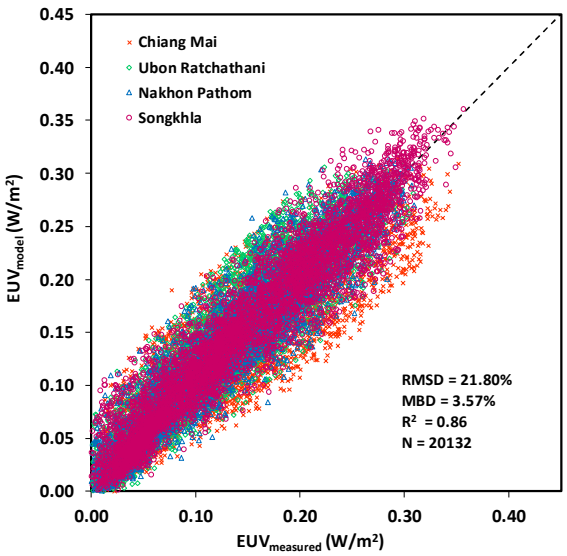

Fig. 7 Comparing erythemal ultraviolet irradiance from mapping model (EUV_{model}) and ground-based measurement ($EUV_{measued}$) for all stations.

Chiang Mai exhibited the highest RMSD at 26.09%, indicating greater variability between modeled and measured values, possibly due to complex topography and seasonal aerosol variations from biomass burning events, which may not be fully captured by visibility data. The MBD of -2.41% also suggests a slight underestimation by the model in this region.

For Ubon Ratchathani, the RMSD was 23.47%, with a positive MBD of 8.22%, indicating a moderate overestimation of EUV irradiance by the model. This could be attributed to frequent cloud cover and fluctuating humidity levels during the wet season, which may introduce uncertainty in satellite-derived cloud index values. Nakhon Pathom showed improved agreement between observed and modeled values, with a lower RMSD of 18.24% and an MBD of 3.80%. Its relatively flat terrain and moderate atmospheric variability may contribute to the model's better performance in this central region. Songkhla achieved the lowest RMSD 18.01% among all stations, reflecting strong model reliability. However, the MBD of 4.57% points to a consistent slight overestimation. The province's persistent cloud cover and humid tropical conditions may reduce variability, allowing the model to perform more consistently, though some fine-scale cloud features might still contribute to bias.

When considering the overall model performance across all four stations, the average RMSD was approximately 21.95%, and the average MBD was around 3.55%. These results demonstrate that the semi-empirical model maintains a relatively high level of accuracy and consistency in estimating hourly EUV irradiance under varying atmospheric and geographical conditions.

4.2 Modified Model Validation

As an alternative for stations with available AOD measurements, modified model (Eq. 6) can be applied to enhance the accuracy of EUV estimation. The validation results are presented in the following Fig. 8.

Fig. 8 illustrates the comparison between modeled and measured hourly EUV irradiance using the modified model that incorporates AOD for the four stations. The inclusion of AOD as an additional parameter significantly improved the model's performance, particularly in regions where aerosols play a major role in attenuating UV radiation.

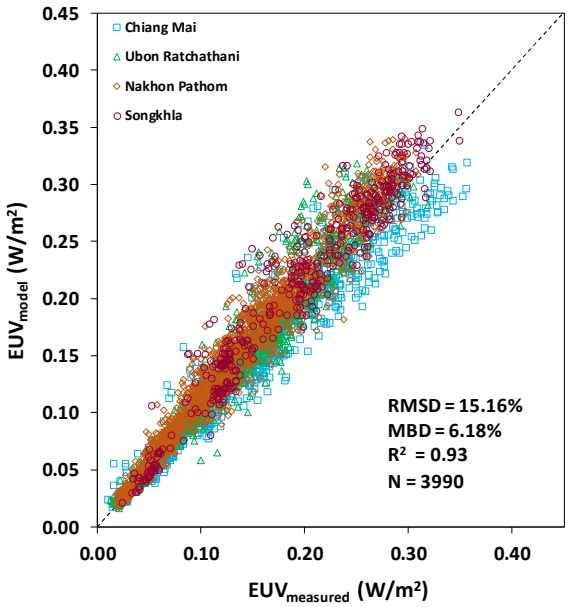

Fig. 8 Comparing erythemal ultraviolet irradiance from mapping model (EUV_{model}) and ground-based measurement ($EUV_{measued}$) for all stations.

Table 5 Performance comparison between the models derived from Eq. 5 and Eq. 6.

station	Eq.5			Eq. 6		
	RMSD (%)	MBD (%)	R^2	RMSD (%)	MBD (%)	R^2
Chiang Mai	26.09	-2.40	0.75	14.17	-1.80	0.92
Ubon Ratchathani	23.47	8.22	0.84	15.13	6.30	0.94
Nakhon Pathom	18.24	3.80	0.90	17.40	11.69	0.95
Songkhla	18.01	4.57	0.90	13.94	8.54	0.93
all	21.80	3.57	0.86	15.16	6.18	0.93

As shown in Table 5, the root mean quare difference and mean bias difference values for all stations decreased when using modified model (Eq.6) compared to the original model (Eq.5). Chiang Mai exhibited the most substantial improvement, with RMSD reducing from 26.09% to 14.17%, and the coefficient of determination (R^2) increasing from 0.75 to 0.92. This suggests that including AOD better captures aerosol-related variability, which is prominent in northern Thailand due to seasonal biomass burning. Ubon Ratchathani also showed marked improvement, with RMSD dropping from 23.47% to 15.13%, and R^2 rising from 0.84 to 0.94. In this region, where fluctuating humidity and cloud cover are common, the AOD parameter complements the cloud index in accounting for UV attenuation. Nakhon Pathom, while the RMSD improvement was modest (from 18.24% to 17.40%), the R^2 still improved slightly, reflecting more consistent estimation under stable central climatic conditions. Similarly, in Songkhla, the RMSD decreased from 18.01% to 13.94%, and R^2 increased from 0.90 to 0.93, indicating improved accuracy even in a humid, tropical environment with frequent cloud cover.

Overall, the average RMSD across all stations decreased from 21.80% (Eq.5) to 15.16% (Eq.6), and the average MBD increased slightly from 3.57% to 6.18%, indicating a mild positive bias. However, the improvement in correlation (R^2 increasing from 0.86 to 0.93) demonstrates that the inclusion of AOD enhances the model's predictive capacity.

These results affirm that aerosol effects, particularly in regions impacted by biomass burning or industrial pollution, must be directly considered in EUV estimation models. The modified model provides a more robust framework for future applications in UV forecasting, public health planning, and environmental monitoring.

Among the atmospheric parameters considered, the solar zenith angle exhibited the most significant influence on EUV irradiance, as expected due to its direct relationship with solar geometry and atmospheric path length. This finding aligns with previous studies, such as Cordero et al. (2008) [37], which confirmed the exponential dependence of UV radiation on the cosine of the solar zenith angle.

The baseline model (Eq.5), which integrates solar zenith angle, cloud index, visibility, and total column ozone, demonstrated satisfactory performance across all four stations, with an average RMSD of 21.80% and a coefficient of determination (R^2) of 0.86. These results indicate that the model is both practical and applicable in areas where aerosol data are unavailable, offering a low-cost alternative for estimating EUV irradiance based on routinely measured meteorological and satellite parameters.

To further enhance model accuracy, aerosol optical depth (AOD) was introduced as an additional parameter in Eq. 6 and applied at stations where AOD data were available. The inclusion of AOD resulted in a notable improvement in model performance. As summarized in Table 5 and illustrated in Fig. 8, the average RMSD decreased significantly to 15.16%, and the coefficient of determination (R^2) increased to 0.93. Chiang Mai—where seasonal biomass burning leads to elevated levels of fine-mode aerosols—exhibited the most substantial improvement, with RMSD decreasing from 26.09% to 14.17% and R^2 rising from 0.75 to 0.92. Similarly, Ubon Ratchathani, which is often affected by fluctuating humidity and cloud cover during the monsoon season, also showed enhanced estimation accuracy with the integration of AOD. This observation is consistent with previous studies that report high aerosol loading in northern Thailand during the biomass burning season [42-43]

Although the improvement in Nakhon Pathom and Songkhla was less dramatic, both stations still benefited from increased model precision, particularly in capturing short term fluctuations in atmospheric transparency. These findings underscore the importance of including aerosol-related parameters in radiative transfer modeling, especially in regions prone to particulate pollution or seasonal haze.

Collectively, the findings indicate that the baseline model (Eq.5) remains a robust and versatile tool for nationwide application, particularly in areas where detailed aerosol measurements are unavailable. In contrast, the modified model (Eq.6) demonstrates superior accuracy and should be prioritized in research or operational settings where high-resolution AOD data—such as those from AERONET or satellite-based sources—are accessible. The enhanced performance of the modified model highlights the importance of accounting for site-specific atmospheric conditions in UV irradiance modeling and underscores the potential benefits of expanding ground-based AOD monitoring networks to improve EUV estimation in Thailand and other tropical regions.

4.3 Strengths and Limitations of the Model

The developed semi-empirical models, both baseline and AOD-enhanced versions, demonstrate several practical strengths. First, the models are relatively simple and computationally efficient, making them well-suited for integration into large-scale or real-time environmental monitoring systems. By using routinely available satellite-

derived parameters—such as solar zenith angle, cloud index, and visibility—the models provide a cost-effective solution for estimating hourly erythemal UV (EUV) irradiance without requiring sophisticated instrumentation.

Another strength lies in the model's flexibility across different geographic regions. The inclusion of multiple monitoring stations representing diverse climatic zones—ranging from the relatively dry inland region of Chiang Mai to the humid coastal area of Songkhla—demonstrates the model's generalizability. Moreover, the enhanced model incorporating aerosol optical depth (AOD) significantly improves performance, especially under conditions of high aerosol loading, such as during biomass burning events in northern Thailand.

Despite these strengths, the models also have limitations. The baseline model tends to underperform in regions or seasons characterized by high aerosol concentrations or complex atmospheric conditions, as it does not account for aerosol-specific attenuation. Although the inclusion of AOD improves accuracy, the availability of high-resolution, real-time AOD data remains a constraint in some regions. Additionally, visibility, used as a surrogate for AOD in the baseline model, may be influenced by local meteorological noise and non-aerosol-related phenomena, introducing potential bias in the estimates.

Finally, the models are deterministic and assume consistent behavior across atmospheric layers and conditions. They do not account for vertical aerosol distribution, cloud type variability, or other dynamic interactions such as photochemical reactions, which could affect UV transmittance. As such, further improvements may involve integrating machine learning techniques and high-resolution temporal datasets to better capture the nonlinearities and interactions in atmospheric parameters.

5. Conclusions

In this study, a semi-empirical model was successfully developed to estimate hourly erythemal ultraviolet *(*EUV*)* irradiance across Thailand using satellite and meteorological data*.* The initial model (Eq.5) integrated four parameters*:* solar zenith angle, cloud index, visibility, and total column ozone*.* It demonstrated a strong correlation with ground-based measurements, with an overall RMSD of 21.8*%* and MBD of 3.57*%.* To enhance accuracy, a modified version of the model (Eq.6) was formulated by incorporating AOD at stations where such data were available*.* The validation results indicated that Eq.6 significantly improved performance across all stations, reducing the average RMSD to 15.16*%* and increasing the overall R^2 to 0.93*.* The greatest improvement was observed in Chiang Mai, where AOD played a critical role due to seasonal biomass burning and fine particulate matter*.* These findings confirm that including AOD as a parameter improves model accuracy, especially in areas affected by aerosol variability*.* The model's simplicity and reliance on readily available data make it suitable for real-world applications in UV risk management, public health planning, and environmental monitoring*.*

Future research should explore broader integration of AOD using satellite products and PM2.5 datasets to extend the model's applicability on a nationwide scale. To further enhance predictive performance, seasonal variability should be incorporated, and advanced machine learning approaches, such as artificial neural networks (ANN), should be employed to improve resolution under complex atmospheric conditions. Additionally, future studies should incorporate post-2021 datasets to update model parameters and better capture recent trends in atmospheric variability and aerosol dynamics.

Acknowledgements

The authors would like to thank Christian University of Thailand for the funding (Grant No. 006/2022) of this research. We are also grateful to the Thai Meteorological Department for providing meteorological data.

References

[1] Gueymard, C. A., The sun's total and spectral irradiance for solar energy applications and solar radiation models. *Solar Energy.* 76 (2004) 423-453, doi: https://doi.org/10.1016/j.solener.2003.08.039.

[2] Roshan, D. R., Koc, M., Abdallah, A., Martin-Pomares, L., Isaifan, R. and Fountoukis, C., UV Index Forecasting under the Influence of Desert Dust: Evaluation against Surface and Satellite-Retrieved Data. *Atmosphere*. 11 (2020) 96, doi: https://doi.org/10.3390/atmos11010096.

[3] Wu, J., Qin, W., Wang, L. Hu, B., Song, Y. and Zhang, M., Mapping clear-sky surface solar ultraviolet radiation in China at 1 km spatial resolution using Machine Learning technique and Google Earth Engine. *Atmospheric Environment*. 286 (2022),119219, doi: https://doi.org/10.1016/j.atmosenv.2022.119219.

[4] Farman, J. C., Gardiner, B. and Shanklin, J., Large losses of total zone in Antarctic reveal seasonal ClO_x/NO_x interaction, *Nature*. 315 (1985) 207-210, doi: http://dx.doi.org/10.1038/315207a0.

[5] Varotsos, C. A., Efstathiou, M. N. and Christodoulakis, J., The lesson learned from the unprecedented ozone hole in the Arctic in 2020; A novel nowcasting tool for such extreme events. *Journal of Atmospheric and Solar-Terrestrial Physics.* 207 (2020) 105330, doi: https://doi.org/10.1016/j.jastp.2020.105330.

[6] Bais, A. F., Lucas, R. M., Bornman, J. F., Williamson, C. E., Sulzberger, B., Austin, A. T., Wilson, S. R., Andrady, A. L., Bernhard, G., McKenzie, R. L., Aucamp, P. J., Madronich, S., Neale, R. E., Yazar, S., Young, A. R., de Gruijl, F. R., Norval, M., Takizawa, Y., Barnes, P. W., Robson, T. M., Robinson, S. A., Bailaré, C. L., Flint, S. D., Neale, P. J., Hylander, S., Rose, K. C., Wängberg, S. -Å., Häder, D. -P., Worrest, R. C., Zepp, R. G., Paul, N. D., Cory, R. M., Solomon, K. R., Longstreth, J., Pandey, K. K., Redhwi, H. H., Torikai, A. and Heikkilä A. M., Environmental effects of ozone depletion, UV radiation and interactions with climate change: UNEP Environmental Effects Assessment Panel, update 2017. *Photochem Photobiol Sci*. 17 (2018) 127-179, doi: https://doi.org/10.1039/c7pp90043k.

[7] Bernhard, G. H., Neale, R. E., Barnes, P. W., Neale, P. J., Zepp, R. G., Wilson, S. R. Andrady, A. L., Bais, A. F., McKenzie, R. L., Aucamp, P. J., Young, P. J., Liley, J. B., Lucas, R. M., Yazar, S., Rhodes, L. E., Byrne, S. N., Hollestein, L. M., Olsen, C. M., Young, A. R., Robson, T. M., Bornman, J. F., Jansen, M. A. K., Robinson, S. A., Ballaré, C. L., Williamson, C. E., Rose, K. C., Banaszak, A. T., Häder, D. -P, Hylander, S., Wängberg, S. -Å., Austin, A. T., Hou, W. -C., Paul, N. D., Madronich, S., Sulzberger, B., Solomon, K. R., Li, H., Schikowski, T., Longstreth, J., Pandey, K. K., Heikkilä, A. M. and White, C. C., Environmental effects of stratospheric ozone depletion, UV radiation and interactions with climate change: UNEP Environmental Effects Assessment Panel, update 2019. *Photochem Photobiol Sci.* 19 (2020) 542-584, doi: https://doi.org/10.1039/d0pp90011g.

[8] Holick, M. F., Resurrection of vitamin D deficiency and rickets. *The Journal of Clinical Investigation.* 116 (2006) 2062-2072, doi: https://doi.org/10.1172/JCI29449.

[9] Roberts, J. E., Ultraviolet radiation as a risk factor for cataract and macular degeneration. *Eye & Contact Lens: Science & Clinical Practice*. 37 (2011) 246-249, doi: https://doi.org/10.1097/ICL.0b013e31821cbcc9.

[10] Hu, B., Wang, Y. and Liu, G., Infuences of the clearness index on UV solar radiation for two locations in the Tibetan Plateau-Lhasa and Haibei. *Advances in Atmospheric Sciences.* 25 (2008) 885-896, doi: https://doi.org/10.1007/s00376-008-0885-8.

[11] Choosri, P., Janjai, S., Nunez, M., Buntoung, S. and Chanalert, W., Development of a method for mapping monthly average hourly diffuse erythemal ultraviolet radiation. *Journal of Atmospheric and Solar-Terrestrial Physics*. 161 (2017) 19-27, doi: https://doi.org/10.1016/j.jastp.2017.06.003.

[12] Lamy, K., Portafaix, T., Brogniez, C., Godin-Beekmann, S., Bencherif, H., Morel, B. Pazmino, A., Metzger, J. M., Auriol, F., Deroo, C., Duflot, V., Goloub, P., and Long, C. N., Ultraviolet radiation modelling from ground-based and satellite measurements on Reunion Island, southern tropics. *Atmospheric Chemistry and Physics*. 18 (2018) 227–246, doi: https://doi.org/10.5194/acp-18-227-2018.

[13] García-Rodríguez, S. García-Rodríguez, A., Granados-López, D., García, I. and Alonso-Tristán, C., Ultraviolet Erythemal Irradiance (UVER) under Different Sky Conditions in Burgos, Spain: Multilinear Regression and Artificial Neural Network Models. *Applied Sciences*. 13 (2023) 10979, doi: https://doi.org/10.3390/app131910979.

[14] Buntoung, S., Laiwarin, P., Pattarapanitchai, S., Masiri, I., Wattan, R., Tohsing, K., Kangwanwit, W. and Janjai, S., Development of maps for monthly average hourly vitamin D–weighted solar ultraviolet radiation over Thailand using a semi-empirical model with ground-based and satellite-based inputs. *Theoretical and Applied Climatology*. 155 (2024) 2499-2507, doi: https://doi.org/10.1007/s00704-023-04799-1.

[15] Lean, J. L., Modelling solar UV irradiance variability. *Advances in Space Research.* 8 (1988) 85-94, doi: https://doi.org/10.1016/0273-1177(88)90176-7.

[16] Díaz, J. P., Expósito, F. J., Arbelo, M., Hernández-Leal, P. A., Torres, C. and Carreño, V., Radiative transfer modeling in the UV-VIS region with the presence of Saharan mineral desert aerosols. *Advances in Space Research.* 26 (2000) 1009-1012, doi: https://doi.org/10.1016/S0273-1177(00)00048-X.

[17] McKenzie, R., Smale, D. and Kotkamp, M., Relationship between UVB and erythemally weighted radiation. *Photochem Photobiol Sci*. 3 (2004) 252-256, doi: https://doi.org/10.1039/b312985c.

[18] Na, H. R., Heisler, G. M., Nowak, D. J. and Grant, R. H., Modeling of urban trees' effects on reducing human exposure to UV radiation in Seoul, Korea. *Urban Forestry & Urban Greening.* 13 (2014) 785-792, doi: https://doi.org/10.1016/j.ufug.2014.05.009.

[19] Escobedo, J. F., Gomes, E. N., Oliveira, A. P. and Soares, J., Modeling hourly and daily fractions of UV, PAR and NIR to global solar radiation under various sky conditions at Botucatu, Brazil. *Applied Energy*. 86 (2009) 299-309, doi: https://doi.org/10.1016/j.apenergy.2008.04.013.

[20] Leal, S. S., Tíba, C. and Piacentini, R., Daily UV radiation modeling with the usage of statistical correlations and artificial neural networks. *Renewable Energy*. 36 (2011) 3337-3344, doi: https://doi.org/10.1016/j.renene.2011.05.007.

[21] Prasad, S. S., Deo, R. C., Downs, N. J., Casillas-Pérez, D., Salcedo-Sanz, S. and Parisi, A. V., Very short-term solar ultraviolet-A radiation forecasting system with cloud cover images and a Bayesian optimized interpretable artificial Intelligence model. *Expert Systems with Applications*. 236 (2024) 121273, doi: https://doi.org/10.1016/j.eswa.2023.121273.

[22] Kottek, M., Grieser, J., Beck, C., Rudolf, B. and Rubel, F., World map of the Köppen-Geiger climate classification updated. *Meteorologische Zeitschrift.* 15 (2006) 259–263, doi: https://doi.org/10.1127/0941-2948/2006/0130.

[23] Srivanit, M. and Iamtrakul, P., Spatial patterns of greenspace cool islands and their relationship to cooling effectiveness in the tropical city of Chiang Mai, Thailand. *Environ Monit Assess.* 191 (2019) 1-16, doi: https://doi.org/10.1007/s10661-019-7749-9.

[24] Khamkaew, C., Chantara, S. and Wiriya, W., Atmospheric PM2. 5 and its elemental composition from near source and receptor sites during open burning season in Chiang Mai, Thailand. *International Journal of Environmental Science and Development.* 7 (2016) 436-440, doi: https://doi.org/10.7763/IJESD.2016.V7.815.

[25] Thongsame, W., Henze, D. K., Kumar, R., Barth, M. and Pfister, G., Evaluation of WRF-Chem PM2.5 simulations in Thailand with different anthropogenic and biomass-burning emissions. *Atmospheric Environment: X*. 23 (2024) 1-20, doi: https://doi.org/10.1016/j.aeaoa.2024.100282.

[26] Saelim, R., Musikasuwan, S. and Chetae, N., Land surface temperature changes in Songkhla, Thailand from 2001 to 2018. *Naresuan University Journal: Science and Technology.* 28 (2020) 39-45, doi: https://doi.org/10.14456/nujst.2020.24.

[27] Noppradit, P., Pradit, S., Muenhor, D., Doungsuwan, N., Whangsani, U., Sama, N. and Towatana, P., Investigation of 37 years weather record and its relation to human health: a case study in Songkhla province, southern Thailand. *International Journal of Agricultural Technology*. 17 (2021) 1507-1520.

[28] Liang, Y., Che, H., Gui, K., Zheng, Y., Yang, X., Li, X., Liu, C., Sheng, Z., Sun, T. and Zhang, X., Impact of biomass burning in South and Southeast Asia on background aerosol in Southwest China. *Aerosol and Air Quality Research.* 19 (2019) 1188–1204, doi: https://doi.org/10.4209/aaqr.2018.08.0324.

[29] Dejchanchaiwong, R., Tekasakul, P., Morris, J., Ingviya, T., Latif, M. T., Amil, N., Hata, M., Furuuchi, M., Dominick, D. and Malinee, R. in *Environmental Nanopollutants: Sources, Occurrence, Analysis and Fate: Biomass Burning in Southeast Asia and Influences on Atmospheric Nanoparticle,* Ch. 3, The Royal Society of Chemistry, (2022) 49-81, doi: https://doi.org/10.1039/9781839166570-00049.

[30] Fan, W., Li, J., Han, Z., Wu, J., Zhang, S., Zhang, C. and Li, J., Impacts of biomass burning in Southeast Asia on aerosols over the low-latitude plateau in China: An analysis of a typical pollution event. *Frontiers in Environmental Science.* 11 (2023) 1-18, doi: https://doi.org/10.3389/fenvs.2023.1101745.

[31] Webb, A., Gröbner, J. and Blumthaler, M., *A practical guide to operating broadband instruments measuring erythemally weighted irradiance.* Report No. EUR22595, EU Publications Office, (2006) 1-17.

[32] Webb, A., Gardiner, B. G., Martin, T. J., Leszcynski, K., Metzdorf, J. and Mohnen, V. A. *Guidelines for site quality control of UV monitoring*. Report No. WMO/GAW, 126, World Meteorological Organization (WMO), (1998).

[33] Seckmayer, G., Basis, A., Bernhard F., Blumthaler, M., Booth,C. R., Lantz, K. and McKenzie, R. L. *Instruments to Measure Solar Ultraviolet RadiationPart 2: Broadband Instruments Measuring Erythemally WeightedSolar Irradiance*. Report No. WMO/GAW, 164, World Meteorological Organization (WMO), (2007).

[34] Ångström, A., On the atmospheric transmission of sun radiation and on dust in the air. *Geografiska Annaler*. 2 (1929) 156-166.

[35] Janjai, S., Kumharn, W. and Laksanaboonsong, J., Determination of Angstrom's turbidity coefficient over Thailand. *Renewable Energy.* 28 (2003) 1685-1700, doi: https://doi.org/10.1016/S0960-1481(03)00010-7.

[36] Iqbal, M. *An introduction to solar radiation*. 1st edn., Academic Press, 1983.

[37] Cano, D., Monget, J. M., Albuisson, M., Guillard, H., Regas, N. and Wald, L., A method for the determination of the global solar radiation from meteorological satellite data. *Solar Energy*. 37 (1986) 31–39, doi: https://doi.org/10.1016/0038-092X(86)90104-0.

[38] Eniola, V., Suriwong, T., Sirisamphanwong, C. and Ungchittrakool, K., Hour-ahead Forecasting of Photovoltaic Power Output based on Hidden Markov Model and Genetic Algorithm. *International Journal of Renewable Energy Research.* 9 (2019) 933-943, doi: https://doi.org/10.20508/ijrer.v9i2.9348.g7659.

[39] Adeyemi, K. O., Eniola, V., Kalu-Uka, G. M., Zarmi, M., Uthman, M. and Bala, E., Forecasting Photovoltaic Energy Generation Using Multilayer Perceptron Neural Network. *International Journal of Renewable Energy Research.* 12 (2022) 1742-1753, doi: https://doi.org/10.20508/ijrer.v12i4.13306.g8599.

[40] Cordero, R. R., Seckmeyer, G. and Labbe, F., Cosine error influence on ground-based spectral UV irradiance measurements. *Metrologia*. 45 (2008) 406-414, doi: https://doi.org/10.1088/0026-1394/45/4/005.

[41] Weiß, C. H., StatSoft, Inc., Tulsa, OK.: STATISTICA, Version 8. *AStA.* 91 (2007) 339–341, doi: https://doi.org/10.1007/s10182-007-0038-x.

[42] Suriyawong, P., Chuetor, S., Samae, H., Piriyakarnsakul, S., Amin, M., Furuuchi, M., Hata, M., Inerb, M. and Phairuang, W. Airborne particulate matter from biomass burning in Thailand: Recent issues, challenges, and options. *Heliyon*. 9 (2023) 1-14, doi: https://doi.org/10.1016/j.heliyon.2023.e14261.

[43] Bran, S. H., Macatangay, R., Surapipith, V., Chotamonsak, C., Chantara, S., Han, Z. and Li, J., Surface PM2.5 mass concentrations during the dry season over northern Thailand: Sensitivity to model aerosol chemical schemes and the effects on regional meteorology. *Atmospheric Research*. 277 (2022) 1-14, doi: https://doi.org/10.1016/j.atmosres.2022.106303.